Environ Fluid Mech (2009) 9:389–407
DOI 10.1007/s10652-008-9113-4

ORIGINAL ARTICLE

Probability law of concentration in plumes dispersing in an urban area

Eugene Yee

Received: 17 July 2008 / Accepted: 15 October 2008 / Published online: 2 November 2008

Abstract The relationships between various normalized higher-order concentration moments in plumes dispersing in a built-up (urban) environment have been investigated using a large concentration data set obtained in a boundary-layer water channel. This data set consists of measurements of plume dispersion in a number of idealized obstacle arrays (e.g., cubical and non-cubical obstacles in aligned and staggered arrangements with uniform, random and alternating heights). A remarkably robust feature of all the concentration data was the observed collapse of the third- and fourth-order normalized concentration moments on the second-order normalized concentration moment. The data are shown to collapse to a series of universal curves (independent of the geometry of the obstacle array) and these curves were found to be identical to those observed previously for open-terrain plumes. The results imply that the probability law of concentration in a plume dispersing in either a built-up environment or open terrain has a universal form that can be specified by at most two independent parameters. The universal functions representing the relationships between the normalized concentration moments were found to be well modeled (approximated) using a two-parameter clipped-gamma probability law for the concentration. Finally, the clipped-gamma distribution was found to be in very good conformance with the measured probability distribution of concentration for plumes dispersing in a built-up environment.

Keywords Atmospheric diffusion · Concentration fluctuations · Pollutant dispersion · Probability density function · Urban canopy

1 Introduction

Demographic evolution, cultural developments and economic activity have accelerated the formation and growth of cities, resulting in a rising proportion of the population living in urban areas. With this increasing urbanization, there is a growing interest in the development

E. Yee (✉)
Defence R&D Canada – Suffield, Stn Main, P.O. Box 4000, Medicine Hat, AB, Canada T1A 8K6
e-mail: eugene.yee@drdc-rddc.gc.ca

of methodologies for the analysis and assessment of actual or potential hazards associated with the release and dispersion of noxious substances in the urban environment where the population is most concentrated.

The concentration in plumes of noxious pollutants is inherently a random variable, owing to the stochastic nature of the turbulent processes responsible for dispersion in the atmosphere. In consequence, the assessment of hazards associated with an accidental or deliberate release of a toxic material in the urban environment requires a knowledge of the statistical characteristics of the fluctuating plume concentrations [1–4]. The statistical description of the natural random fluctuations in the instantaneous concentration of a plume dispersing in the atmosphere is conveniently summarized in the probability law of concentration. More specifically, in order to investigate and model concentration fluctuation phenomenology, it is useful to know the probability density function (PDF) of concentration which necessarily embodies all the higher-order concentration moments of the stochastic process [5].

The shape and form of the concentration PDF of dispersing plumes in the atmosphere have been studied by numerous investigators [6–13]. All the studies cited here have focused exclusively on plumes dispersing over level, unobstructed terrain. Unfortunately, there is currently a paucity of information concerning the statistical description of concentration fluctuations in plumes dispersing in urban (built-up) areas and, more particularly, the characterization of the shape of the one-point concentration PDF for instantaneous plumes dispersing within urban areas. Nevertheless, a very small number of studies focusing on the elucidation of the statistical characteristics of concentration fluctuations in plumes dispersing in an urban environment have begun to appear [14–17].

In view of the paucity of information on the characteristics of the probability law of concentration in plumes dispersing in a built-up (urban) environment, the objective of this paper is to investigate how the structure of the statistical properties of a plume dispersing through regular arrays of obstacles (as manifested through the higher-order moments of concentration and the concentration probability density function) is modified in comparison to that observed for a plume dispersing over a level, unobstructed terrain.

2 Experimental setup and physical modeling

2.1 Water-channel setup

The comprehensive, high-quality data sets of dispersion of array plumes were obtained from water-channel simulations commissioned by Defence R&D Canada – Suffield and conducted at Coanda Research & Development Corporation's (Burnaby, British Columbia, Canada) boundary-layer water channel. The water-channel facility and the experiments that were carried out are fully described in Hilderman and Chong [18]. As a consequence, only the important details of the experiments that are required for the interpretation of the following data analysis will be presented here.

The experiments were conducted in a re-circulating water channel with a working section of 10 m length, 1.5 m width, and 0.9 m height. The upstream portion of the working section was used to generate a naturally-grown neutrally-stratified rough-walled boundary layer of about 0.3 m thickness. This portion of the water-channel floor was covered with a black-anodized expanded metal mesh of height 4 mm, with a total streamwise length of 6 m. This gave a sufficiently long fetch of uniform surface roughness for the upstream channel flow to develop. After this uniform upstream fetch of expanded metal mesh, the flow then encountered the model obstacle array. Downstream of the obstacle array, the flow encountered a

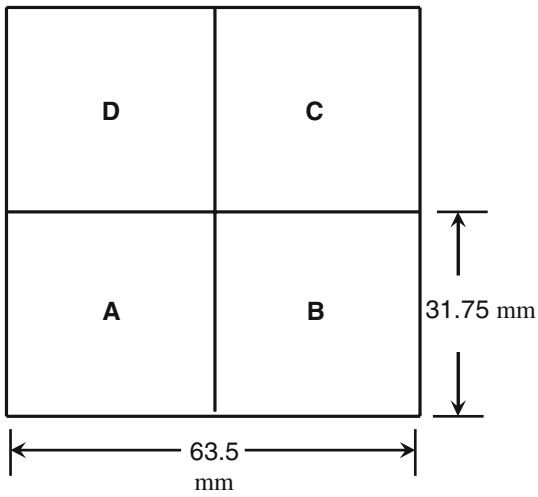

Fig. 1 Basic unit cell used to construct 'urban' obstacle arrays. Obstacles can be placed on any quadrant A, B, C or D of the unit cell

section covered with the same expanded metal mesh that was used for the initial upstream boundary-layer development.

Measurements of the vertical profiles of mean streamwise velocity, $\overline{u}$, streamwise velocity variance, $\sigma_u^2 \equiv \overline{u'^2}$, and shear stress, $\tau \equiv \overline{u'w'}$, were made using a 4-beam, 2-component fibre-optic laser Doppler velocimeter (LDV) within the equilibrium (fully-developed) boundary layer upstream of the obstacle array.[1] The measurements showed that these profiles of velocity statistics were homogeneous to within $\pm 5\%$ in the spanwise direction across the channel. The boundary-layer thickness, δ, taken to be the height where the mean wind speed reached 99% of the free-stream value, was found to be 275 mm. At this point, the mean wind speed $\overline{u}_\delta$ was 0.375 m s^{-1}. The friction velocity, $u_{*0} \equiv (\overline{u'w'})^{1/2}$, in the fully-developed (undisturbed) flow upstream of the model obstacle array was 0.0255 m s^{-1}.

2.2 Obstacle arrays

Five different types of obstacle arrays were used in this study. The obstacle arrays were composed of cubes and/or cuboids (rectangular blocks), constructed from Lego^{TM} blocks. These obstacle arrays were constructed from a square repeating unit cell (63.5 mm $\times$ 63.5 mm) shown in Fig. 1. The unit cell was divided into 4 quadrants labelled A, B, C and D. Each cube or rectangular block of the array had a square cross section with a side length $H = 31.75$ mm. An obstacle can be placed on any one of the 4 quadrants in the unit cell. The obstacle arrays were constructed from a 16 $\times$ 16 unit cell array layout placed on a Lego^{TM} baseplate.

Schematic drawings of the obstacle arrays constructed using cubes and/or cuboids are shown in Fig. 2. For the arrays of aligned obstacles, the obstacles were placed in quadrant A of each unit cell of the array. For the array of staggered obstacles, the obstacles were placed in either quadrant A or B of each unit cell, in accordance to whether the obstacle row number (in the streamwise or flow direction) was odd or even, respectively.

[1] Overbars and primes denote time averages and departures therefrom; and, (u, v, w) are the instantaneous velocities in the streamwise (x), spanwise (y) and vertical (z) directions, respectively.

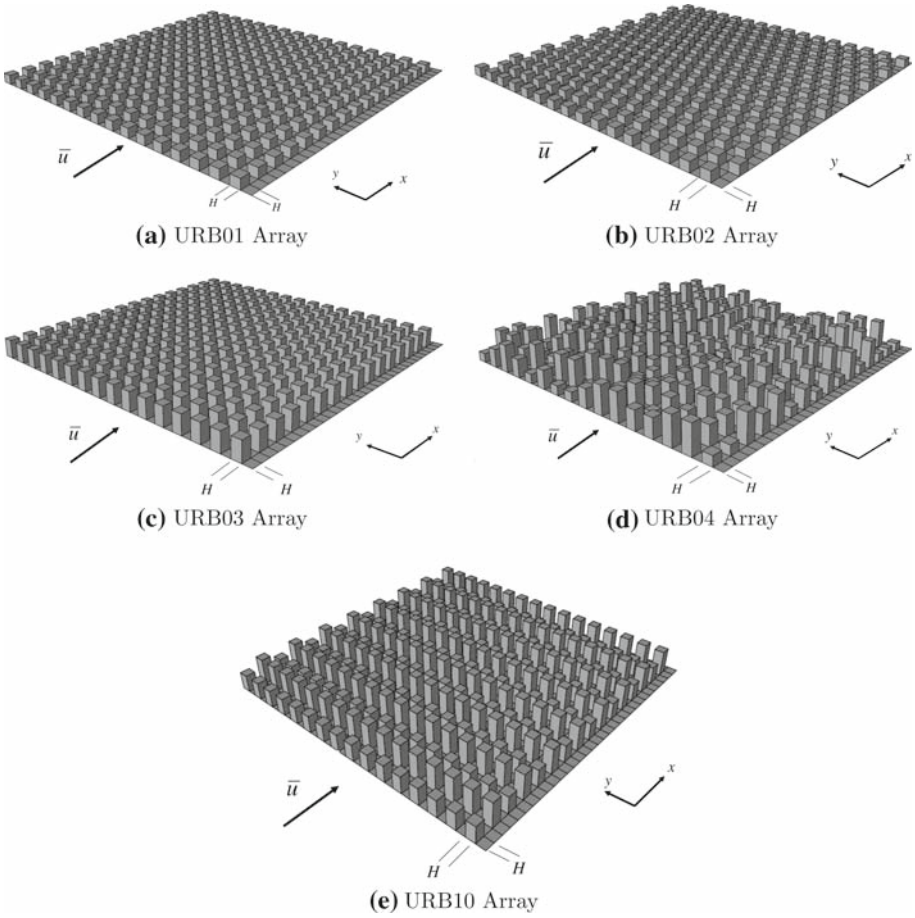

Fig. 2 Schematics of five idealized obstacle arrays. The positive x- and y-axes correspond to the streamwise and spanwise (cross-stream) directions, respectively. URB01 and URB02 are aligned and staggered arrays of cubes with side length H, respectively; URB03 is an aligned array of cuboids, each with a square cross-section of side length H and a height of $2H$; URB04 is an aligned array of random-height cuboids, each with a square cross-section of side length H and heights of either H, $2H$, or $3H$ chosen randomly; and, URB10 is an aligned array of alternating-height cuboids, each with a square cross-section of side length H and heights of $2H$ or $3H$ in alternating sequence

Each of the obstacle arrays had a plan area index $\lambda_p = 0.25$.[2] The first obstacle array used in this study is shown in Fig. 2a and corresponds to an aligned array of 31.75-mm cubes with a frontal area index of 0.25 (URB01). The second obstacle array, exhibited in Fig. 2b, consists of 31.75-mm cubes arranged in a regular staggered pattern with a frontal area index of 0.25 (URB02). The third obstacle array, displayed in Fig. 2c, is an aligned array of rectangular blocks with square cross-section of side length H and height of $2H$ to give an array with a frontal area index of 0.5 (URB03). Fig. 2d shows the fourth obstacle array,

[2] The frontal area index of an obstacle array is defined as $\lambda_f \equiv \langle A_f/A_L \rangle$ (the angled brackets are used to denote an average over all unit cells in the array), where A_f is the frontal (windward) area of an obstacle and A_L is the lot area (surface area of a unit cell within which an obstacle sits in the array). The plan area index is defined as $\lambda_p = \langle A_p/A_L \rangle$, where A_p is the plan (floor) area of an obstacle.

which corresponds to an aligned array of obstacles (cubes or rectangular blocks) with square cross-section H whose heights have been randomly chosen as $H, 2H$, or $3H$ (URB04). Finally, the fifth obstacle array is shown in Fig. 2e, and consists of an aligned array of rectangular blocks with alternating rows of blocks having heights of $2H$ and $3H$, giving a frontal area index of 0.625 (URB10).

2.3 Plume dispersion measurements

For the water-channel simulations involving the five obstacle arrays summarized above, the point source used for the release of the tracer consisted of a vertical stainless steel tube (with an inner diameter of 2.8 mm and an outer diameter of 3.1 mm). The source emitted a sodium fluorescein dye tracer at a constant flow rate of 12×10^{-3} l min^{-1} with low discharge momentum (weak vertical jet). For arrays URB01 (Fig. 2a), URB02 (Fig. 2b), URB03 (Fig. 2c) and URB10 (Fig. 2e), the point source was located at ground level at two different positions: namely, at the center of quadrant D behind an obstacle in a spanwise-oriented street canyon and at the center of quadrant C between two columns of obstacles in a streamwise-oriented street canyon (for the aligned arrays URB01, URB03 and URB10[3]) or in front (on the windward side) of an obstacle (for the staggered array URB02[4]). These sources were located in the unit cell lying at the intersection of the first row and eighth column of obstacles (where the rows are numbered in increasing order in the streamwise (or, x-) direction from the leading (windward) edge of the array and the columns are numbered in increasing order in the spanwise (y-) direction from the right-hand side of the array when looking in the flow direction (see Fig. 2)). For array URB04 (Fig. 2d), the point source was located only at the center of quadrant D behind an obstacle in a spanwise-oriented street canyon.

The instantaneous concentration field in the dispersing dye plume was measured using the laser-induced fluorescence (LIF) technique. The LIF concentration measurements were carried out using a line-scan configuration with the line-of-laser light oriented in either a horizontal or vertical direction through the dispersing plume to provide a lateral or vertical profile of the instantaneous plume concentration. The line scans were sampled at 300 Hz. The sampling time for each experiment was 1,000 s, yielding $N = 300,000$ individual line scans per experiment.

For all obstacle arrays except URB03, horizontal line scans through the dispersing array plume were made at a number of different downstream distances from the source, and for each of these downstream locations a number of vertical heights in the plume were sampled. For the URB01 and URB02 arrays (Fig. 2a, b), the horizontal line scans were made at six different downstream locations (rows 2.5, 3.5, 4.5, 6.5, 9.5, and 14.5) and for each of these locations at three different heights (viz., at $z/H = 0.25$, 0.5 and 1.25). Here, "row 2.5" refers to a streamwise location that is centered in the spanwise-oriented street canyon between rows 2 and 3 of the obstacle array, etc. For array URB03 (Fig. 2c), data from vertical line scans were acquired for the dispersing plume along the mean-plume centerline at six downstream distances from the source (rows 2.5, 3.5, 4.5, 6.5, 9.5, and 14.5). Finally, for arrays URB04 and URB10 (Fig. 2d and e, respectively), horizontal line-scan data were acquired at four downstream distances from the source (rows 2.5, 3.5, 4.5 and 9.5), and at each of these locations for three different vertical heights (i.e., at $z/H = 0.5$, 1.25 and 3.25).

[3] More precisely, the source at the center of quadrant C lies at the intersection of a spanwise-oriented and a streamwise-oriented street canyon.

[4] For the staggered array URB02, a streamwise-oriented street canyon does not exist because the presence of an obstacle in quadrant B for every even-numbered row in the array "blocks" the streamwise-oriented passages through the array.

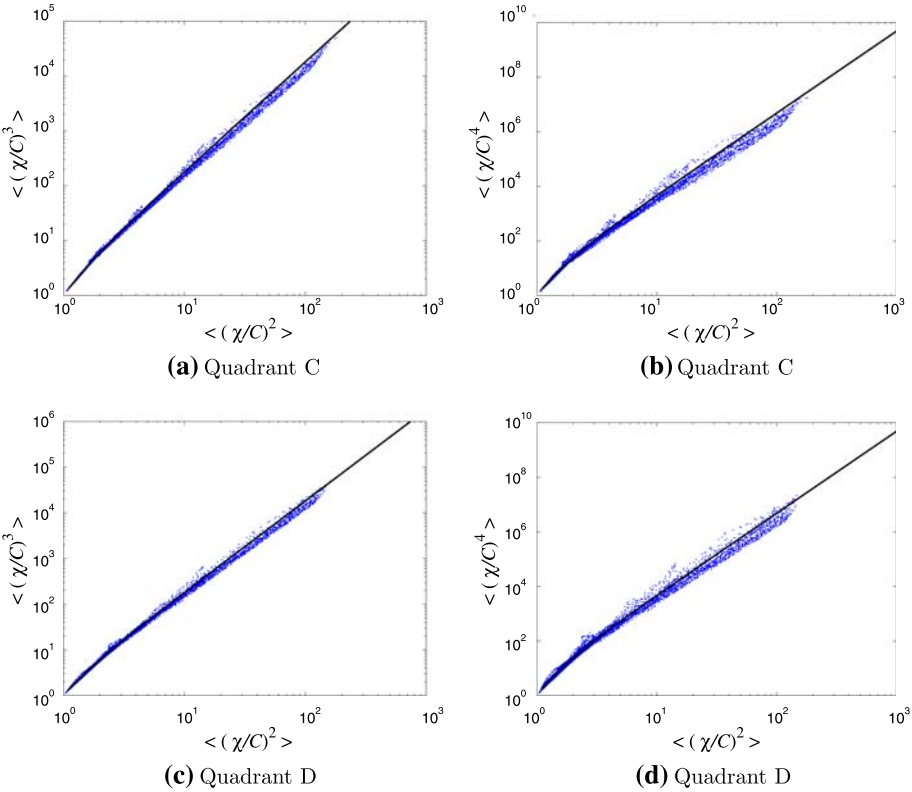

Fig. 3 Scattergrams of third- ($\langle(\chi/C)^3\rangle$) and fourth-order ($\langle(\chi/C)^4\rangle$) normalized concentration moments against the second-order ($\langle(\chi/C)^2\rangle$) normalized concentration moment for the URB01 obstacle array with the source located in quadrants C (in a streamwise-oriented street canyon between two columns of obstacles) and D (behind obstacle in a spanwise-oriented street canyon between two rows of obstacles). For the releases in quadrants C and D, there are 5,510 and 5,799 concentration data points, respectively, in the concentration moment diagrams covering a wide range of positions in the array plume. The plots also include the theoretical curves for the concentration moment relationships predicted by the clipped-gamma distribution (*solid line*)

3 Concentration moment relationships

The concentration time series, extracted from the measurements of plume dispersion through and over the five obstacle arrays described in the previous section, were processed to determine the normalized concentration moments up to order four (viz., we calculated $\langle (\chi/C)^n \rangle$ for $n = 2, 3, 4$ from the concentration data). Here, χ denotes the instantaneous concentration, $\langle \cdot \rangle$ denotes the ensemble average (viz., average over a number of independent realizations of a process[5]) and C is the ensemble-averaged concentration (viz., $C \equiv \langle \chi \rangle$).

Figure 3 exhibits the normalized concentration moment diagrams of $\langle (\chi/C)^n \rangle$ ($n = 3, 4$) plotted against $\langle (\chi/C)^2 \rangle$ on a double-logarithmic scale for the aligned array of cubes (URB01) with the location of the ground-level source positioned in quadrants C and D. Similarly, Fig. 4 displays scatterplots of the third- and fourth-order concentration moments

[5] The concentration time series from a steady and continuous release of a tracer into a statistically stationary flow corresponds to a stationary random process, for which a time average can be considered to be synonymous with an ensemble average.

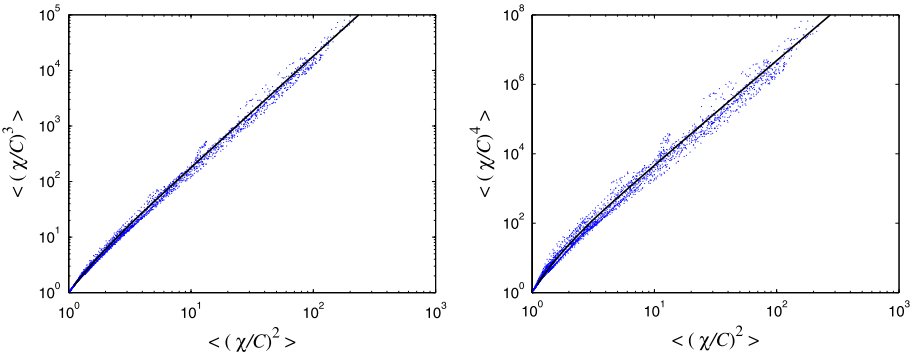

(a) Quadrant D **(b)** Quadrant D

Fig. 4 As Fig. 3 but for URB04, with a release only from a source at the center of quadrant D. In this case, there are 2,749 concentration data points in the concentration moment diagrams

versus the second-order concentration moment for the aligned array of random-height cuboids (URB04). The concentration moment diagrams for the other three obstacle arrays (URB02, URB03, URB10) are very similar to those exhibited for URB01 AND URB04 (and, hence, are not shown owing to space limitations).

It should be noted that there is more scatter in the plots of the normalized moment diagrams at the higher values of $\langle (\chi/C)^2 \rangle$ (corresponding to positions in the plume that are closer to the plume edges) and at higher values of the moment order n. This increased scatter appears to be random, being most likely attributed to increased sampling errors arising from the measurement of concentration nearer the plume edges and/or of higher-order concentration moments.

The points plotted in Figs. 3 and 4 cover different types of obstacle arrays. Even so, each of the scatterplots exhibited here is seen to collapse onto a curve, suggesting that this collapse is a remarkably robust feature of the concentration data. Moreover, the curves representing the collapse of the normalized third- and fourth-order concentration moments on the normalized second-order concentration moment are *universal* in the sense that these curves are the same for each of the obstacle arrays. In other words, the results presented here suggest that $\langle (\chi/C)^3 \rangle = F_3\big(\langle (\chi/C)^2 \rangle\big)$ and $\langle (\chi/C)^4 \rangle = F_4\big(\langle (\chi/C)^2 \rangle\big)$, where $F_3(\cdot)$ and $F_4(\cdot)$ are universal functions that appear to be valid for all forms of obstacle arrays (viz., it appears that these functions are independent of the characteristics of the obstacle array).

This observed collapse suggests that there are strong correlations between the various higher-order (certainly up to order four) and second-order normalized concentration moments, and that these correlations are independent (approximately or better) of the geometrical properties of the obstacle arrays. To see the suggested "universality" of this collapse of the concentration moments more clearly, Fig. 5 displays scatterplots of the third- and fourth-order concentration moments against the second-order concentration moment for all the concentration data (obtained from all five obstacle arrays for all source locations). The collapse of the concentration moments onto a set of universal curves $\langle (\chi/C)^3 \rangle = F_3\big(\langle (\chi/C)^2 \rangle\big)$ and $\langle (\chi/C)^4 \rangle = F_4\big(\langle (\chi/C)^2 \rangle\big)$ that are independent of the geometrical properties of the obstacle array is supported by this result (to within uncertainties in the measurements of the various concentration moments), although the exact (theoretical) forms for the universal functions F_3 and F_4 are unknown at this juncture.[6]

[6] Although the exact functional forms for F_3 and F_4 are unknown and there does not exist a comprehensive theory of turbulence that would allow these forms to be determined rigorously, it will be shown later in this paper that a simple probability model for the concentration can provide very good approximations for F_3 and F_4.

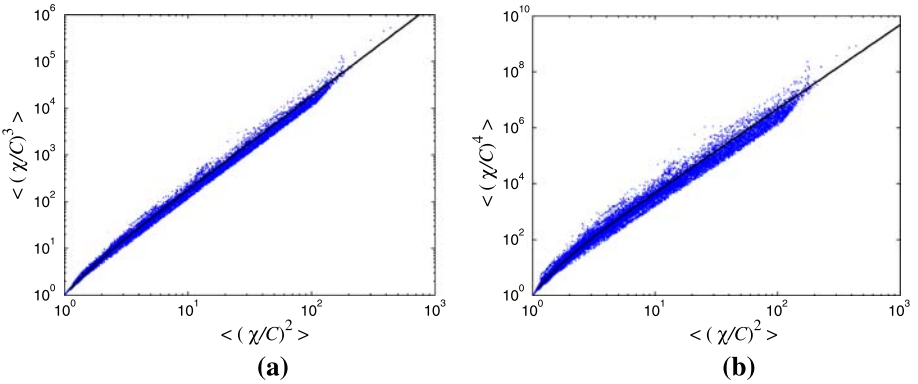

Fig. 5 As Fig. 3 but using all concentration data obtained from the various obstacle arrays investigated. In this case, there are 31,858 concentration data points in the concentration moment diagrams

The results of Figs. 3 and 4 (and similar plots for the other obstacle arrays) provide compelling evidence that the concentration PDF for a plume dispersing in a built-up environment (e.g., arrays of building-like obstacles) can be described by *at most two parameters*. The result of Fig. 5 suggests that a *single* two-parameter probability law of concentration (whatever it is) should be valid for all obstacle arrays (or, perhaps more generally, for an arbitrary built-up environment).[7]

Of course, the functional form for this two-parameter concentration PDF still remains to be determined. Towards this objective, we consider a simple model for the probability law of concentration (whose form is completely specified by two parameters) and examine its flexibility in representing the observed higher-order concentration moment relationships measured in a built-up environment.

4 Model for probability law of concentration

The probability law of concentration provides a concise language for describing the probabilistic properties of the random fluctuations of concentration in a dispersing plume. To this purpose, we propose a model for the one-point concentration PDF $f(c;\mathbf{x})$ at a receptor point $\mathbf{x} \equiv (x, y, z)$, where x, y and z are, respectively, the streamwise, spanwise, and vertical Cartesian coordinates of the point:

$$f(c;\mathbf{x})\,dc \equiv \Pr\{c \le \chi(\mathbf{x}) < c + dc\}, \tag{1}$$

where $\Pr\{\cdot\}$ denotes the "probability that". Here, the right-hand side denotes the probability that the instantaneous concentration $\chi(\mathbf{x})$ falls in the interval of sample space values between c and $c + dc$ for different realizations of the turbulent dispersion of the hazardous plume.

Yee and Chan [19] proposed a left-shifted clipped-gamma distribution for the concentration PDF of plumes dispersing in an unobstructed (open) terrain. This form for the concentration PDF arises from imposing simple closure hypotheses for the conditional pseudo-diffusion

[7] This is implicit in the putative functional relationship between the normalized third- and second-order concentration moments; viz., $\langle (\chi/C)^3 \rangle = F_3\big(\langle (\chi/C)^2 \rangle\big)$. Moreover, the fact that $F_3(\cdot)$ appears to be a universal function suggests that this two-parameter probability law of concentration is also universal (and, applicable perhaps, to any arbitrary built-up environment).

and pseudo-dissipation terms given a fixed concentration level in a dispersing plume. Indeed, the assumption that the conditional pseudo-diffusion and pseudo-dissipation terms for a fixed concentration level are linearly related to the concentration level, leads to a left-shifted and clipped-gamma PDF for the concentration. In this model, the concentration PDF has the following form:

$$f(c;\mathbf{x}) = \left(\frac{c+\lambda}{s}\right)^{k-1} \frac{\exp\big(-(c+\lambda)/s\big)}{s\Gamma(k)} + (1-\gamma)\delta(c), \tag{2}$$

with $k = k(\mathbf{x}) > 0, s = s(\mathbf{x}) > 0, \lambda = \lambda(\mathbf{x}) \geq 0, \gamma = \gamma(\mathbf{x}) \in [0,1]$. Furthermore, $\Gamma(x)$ is the gamma function, $\delta(x)$ is the Dirac delta function and the range for c is $0 \leq c < \infty$. Finally, $\gamma \equiv \Pr\{\chi(\mathbf{x}) > 0\}$ is the intermittency factor that determines the probability of observing a non-zero instantaneous concentration χ at $\mathbf{x}$.

The concentration PDF in Eq. 2 is completely determined by four parameters: namely, γ, k, s and λ. However, only three of these parameters are independent, owing to the fact that the intermittency factor γ is determined uniquely as the area remaining under the gamma PDF curve for $c > 0$ after a left-shift of c by the amount $\lambda \geq 0$; hence,

$$\begin{aligned}\gamma \equiv \gamma(k,s,\lambda) &= \int_{\lambda}^{\infty} \left(\frac{c}{s}\right)^{k-1} \frac{\exp(-c/s)}{s\Gamma(k)}\, dc \\ &= \int_{0}^{\infty} \left(\frac{c+\lambda}{s}\right)^{k-1} \frac{\exp(-(c+\lambda)/s)}{s\Gamma(k)}\, dc \\ &= \frac{\Gamma(k;\lambda/s)}{\Gamma(k)},\end{aligned} \tag{3}$$

where $\Gamma(\nu;x)$ denotes the complementary incomplete gamma function.

Yee and Chan [19] introduced an additional constraint to the left-shifted clipped-gamma distribution in order to obtain a concentration PDF that can be uniquely specified by the information embodied by the two lowest-order moments of concentration; namely, the mean concentration C and the mean-square concentration $\langle \chi^2 \rangle$. Towards this objective, a comprehensive plume concentration data set obtained from the CONFLUX project [20–24] was used to formulate a simple relationship between the normalized mean-square concentration and the plume intermittency factor; namely,

$$\gamma = \min\left(1, \frac{3}{\langle (\chi/C)^2 \rangle}\right). \tag{4}$$

Note that with the parameterization for γ given by Eq. 4, the plume concentration is non-intermittent (viz., $\gamma = 1$) for $\langle (\chi/C)^2 \rangle \in [1,3]$. In this case, the concentration PDF of Eq. 2 reduces to a simple gamma PDF as $\gamma = 1$ and $\lambda = 0$ by virtue of Eq. 3; viz., the concentration PDF reduces to

$$f(c;\mathbf{x}) = \left(\frac{c}{s}\right)^{k-1} \frac{\exp(-c/s)}{s\Gamma(k)}, \tag{5}$$

when $\langle (\chi/C)^2 \rangle \in [1,3]$.

The nth concentration moment (about zero) for the clipped-gamma distribution of Eq. 2 is given by (see, Yee and Chan [19])

$$\langle \chi^n \rangle(\mathbf{x}) = \int_{0^-}^{\infty} c^n f(c;\mathbf{x})\, dc$$
$$= \sum_{j=0}^{n} \binom{n}{j} (-\lambda)^j s^{n-j} \frac{\Gamma(n-j+k;\lambda/s)}{\Gamma(k)}, \quad n \in \mathbb{N}. \tag{6}$$

The model concentration PDF parameters k, s and λ in Eq. 2 can be obtained by application of the method of moments (viz., ensuring that the concentration PDF is consistent with the given first and second moments of concentration) applied to the normalized concentration χ/C. Following this procedure, the identification of the parameters k, s and λ requires the solution of the following system of transcendental equations:

$$\frac{1}{s} = \left(-\frac{\lambda}{s} + k\right)\gamma + \frac{1}{\Gamma(k)}\left(\frac{\lambda}{s}\right)^k \exp(-\lambda/s); \tag{7}$$

$$\left\langle \left(\frac{\chi}{C}\right)^2 \right\rangle = \frac{\big((\lambda/s)\gamma + (-\lambda/s + k + 1)/s\big)}{\big[(-\lambda/s + k)\gamma + (\lambda/s)^k \exp(-\lambda/s)/\Gamma(k)\big]^2}; \tag{8}$$

and

$$\gamma = \min\left(1, 3\left\langle \left(\frac{\chi}{C}\right)^2 \right\rangle^{-1}\right) = \frac{\Gamma(k;\lambda/s)}{\Gamma(k)}. \tag{9}$$

Consequently, for a specified value of $\langle(\chi/C)^2\rangle$, Eqs. 8 and 9 need to be solved for k and λ/s. Next, these values can then be subsequently substituted into Eq. 7 to obtain s, after which the value of λ can be obtained. The system of transcendental equations can be solved numerically to obtain k, s and λ as a function of the normalized second-order concentration moment $\langle(\chi/C)^2\rangle$.

The clipped-gamma PDF of Eq. 2 gives the following explicit form for the cumulative distribution function (CDF) for the concentration (at the receptor point $\mathbf{x}$):

$$F(c;\mathbf{x}) \equiv \Pr\big\{\chi(\mathbf{x}) \le c\big\} = \int_{0^-}^{c} f(c';\mathbf{x})\, dc'$$
$$= 1 - \frac{\Gamma(k;(c+\lambda)/s)}{\Gamma(k)}. \tag{10}$$

The complement of the concentration CDF [or, exceedance distribution function (EDF) for concentration] is simply $\big(1 - F(c;\mathbf{x})\big) \equiv \Pr\big\{\chi(\mathbf{x}) > c\big\}$.

5 Model comparisons with experiments

5.1 Comparison with concentration moments

For comparative purposes, the theoretical relationships between $\langle(\chi/C)^n\rangle$ $(n = 3, 4)$ and $\langle(\chi/C)^2\rangle$ predicted by the clipped-gamma PDF have been superimposed on the scatterplots in Figs. 3 and 4 for two of the obstacles arrays, as well as on scatterplots in Fig. 5 for all the

concentration data. In these figures, the solid line represents the theoretical curve predicted using the proposed clipped-gamma probability law.

The observed concentration moment relationships for plumes dispersing in various built-up environments (as displayed in Figs. 3 and 4) are in excellent conformance with the predictions provided by the clipped-gamma PDF, over the entire range of conditions covered by the concentration data sets. Furthermore, the clipped-gamma PDF predictions for the concentration moment relationships conform well with the measured relationships for all the concentration data exhibited in Fig. 5 (viz., the theoretical curves pass roughly through the center of the spread of points shown in the scatterplots here for most of the range of $\langle(\chi/C)^2\rangle$).[8] Interestingly, Yee and Chan [19] demonstrated that the clipped-gamma PDF provided predictions of concentration moment relationships that were in very good agreement with the measured concentration moment relationships compiled from many experiments conducted in the CONFLUX project (see Fig. 2 in Yee and Chan [19]). These experiments provided plume concentration data for dispersion over level, unobstructed terrain, and included measurements that covered a wide range of plume positions and atmospheric stability conditions.

The results of Fig. 2 in Yee and Chan [19] for dispersion over open terrain and of Figs. 3, 4 and 5 in the current study for dispersion over various built-up environments, strongly suggest that the concentration moment relationships for plumes dispersing in (complex) urban terrain are identical (approximately or better) to those for plumes dispersing in (simple) rural terrain. In this sense, $F_3\left(\langle(\chi/C)^2\rangle\right)$ and $F_4\left(\langle(\chi/C)^2\rangle\right)$ do appear to be universal functions that apply to plume dispersion over any terrain (e.g., open, urban, etc.), and these functions correspond to a remarkably good way to compact all the concentration moment data. Moreover, the precise functional form of these universal functions (although unknown) appear to be well approximated using the clipped-gamma probability law of concentration.

5.2 Comparison with concentration PDF

In this section, we compare the shape of the model probability distribution to the observed concentration data at a number of plume locations for two of the obstacle arrays. To this end, we extract the cumulative and exceedance probability distributions from the array plume concentration data and compare these measured distributions to the model (clipped-gamma) cumulative and exceedance probability distributions. Figure 6 presents measured CDFs of the normalized concentration χ/C obtained at six different downstream locations along the mean-plume centerline at half-canopy height ($z/H = 0.5$) for dispersion in the URB01 obstacle array with the source located in quadrant D. The clipped-gamma distributions, having the same normalized mean-squared concentration $\langle(\chi/C)^2\rangle$ as the measured results, are also exhibited in Fig. 6 for comparison. The clipped-gamma distribution is seen generally to be in very good conformance with the measured concentration CDFs at the various downstream locations. The predictions correctly capture the streamwise evolution of the concentration probability distribution along the mean-plume centerline within the obstacle array. Nevertheless, the agreement between the measured and modeled CDFs appears to be slightly poorer

[8] At large values of $\langle(\chi/C)^2\rangle$, the clipped-gamma PDF predictions for the concentration moments over-predict the measured values. However, it needs to be stressed that these large values of $\langle(\chi/C)^2\rangle$ correspond to receptor locations in the extreme fringes of the plume, implying that the higher-order concentration moments measured here are subject to a much greater sampling error (and uncertainty). Indeed, the limited sampling times used imply that the rare, but large, concentration events in the plume fringes will be under-sampled, leading most probably to an under-estimation of the measured higher-order concentration moments here.

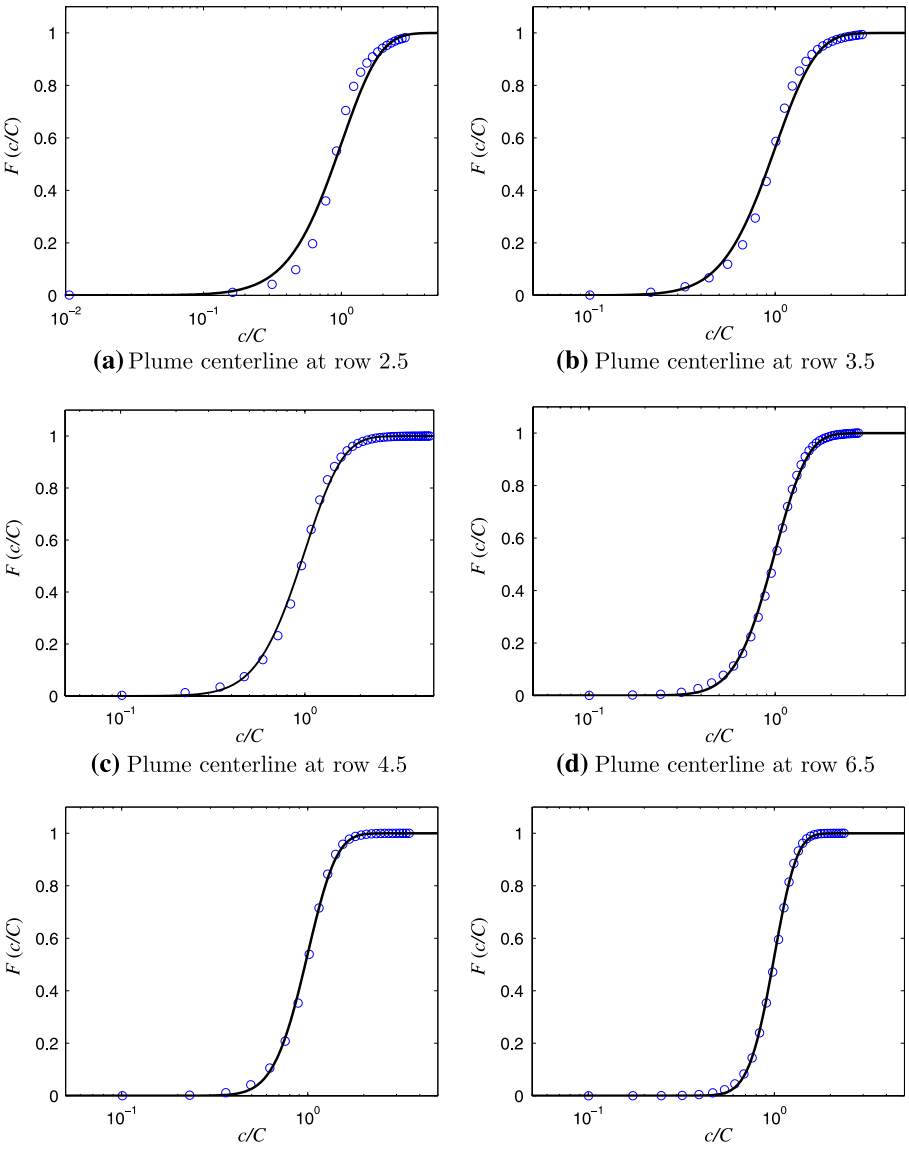

(a) Plume centerline at row 2.5

(b) Plume centerline at row 3.5

(c) Plume centerline at row 4.5

(d) Plume centerline at row 6.5

(e) Plume centerline at row 9.5

(f) Plume centerline at row 14.5

Fig. 6 Cumulative distribution function (CDF), $F(c/C)$, of the normalized concentration measured at various receptor positions at half-canopy height along the centerline of a plume dispersing in the URB01 obstacle array, with the source located in quadrant D. The plot also includes the prediction of the concentration CDF given by the clipped-gamma distribution (*solid line*), which was generated using the observed normalized mean-square concentration $\langle(\chi/C)^2\rangle$ at each plume location

near the source (e.g., at rows 2.5 and 3.5) where the model distributions are seen to be slightly broader than (i.e., does not rise quite as sharply as) the measured distributions.

Generally, for most practical applications, it is the largest peak concentrations that are of greatest interest. Because it is the prediction of the likelihood of extreme events that is important in the hazard assessment of noxious gas releases, it is important to examine the upper

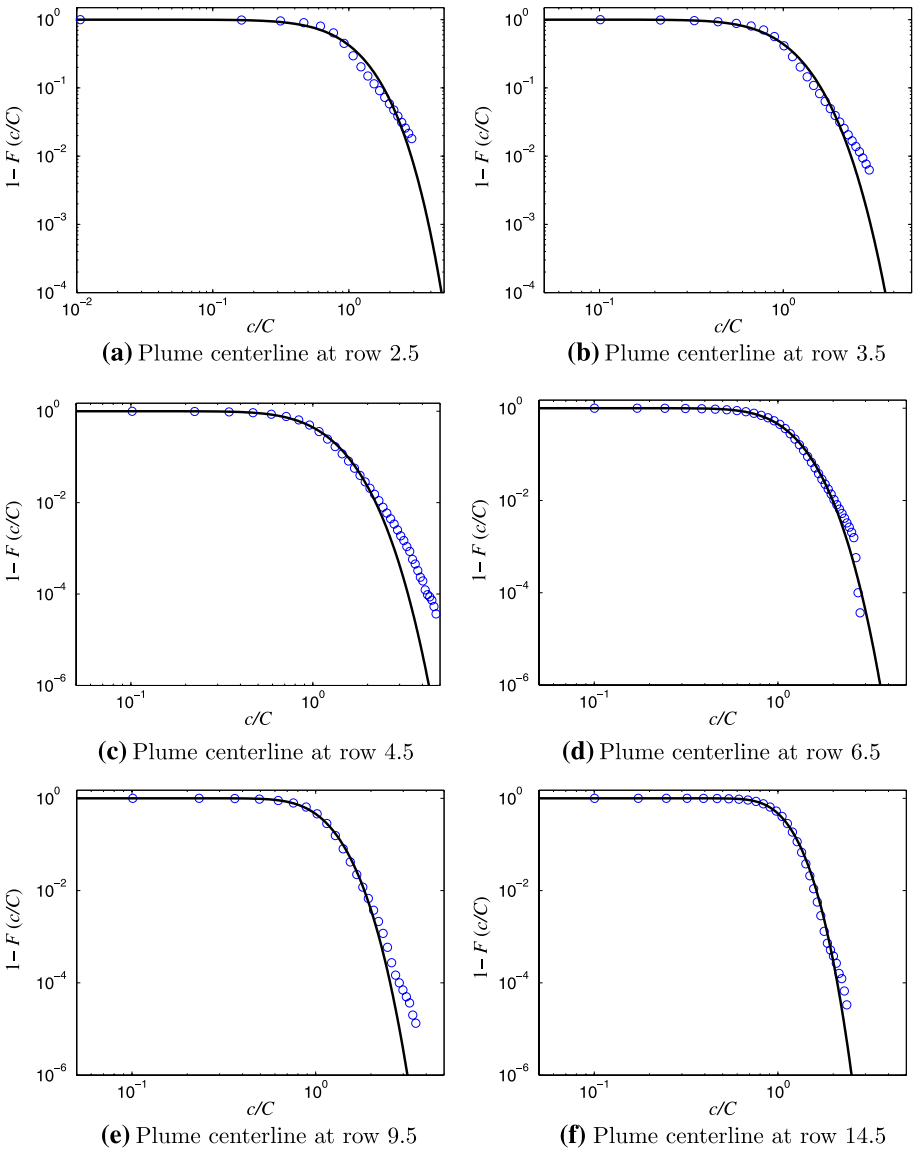

(a) Plume centerline at row 2.5

(b) Plume centerline at row 3.5

(c) Plume centerline at row 4.5

(d) Plume centerline at row 6.5

(e) Plume centerline at row 9.5

(f) Plume centerline at row 14.5

Fig. 7 Exceedance distribution function (EDF), $1 - F(c/C)$, of the normalized concentration measured at various receptor positions at half-canopy height along the centerline of a plume dispersing in the URB01 obstacle array, with the source in quadrant D. The plot also includes the prediction of the concentration EDF given by the clipped-gamma distribution (*solid line*), which was generated using the observed normalized mean-square concentration $\langle(\chi/C)^2\rangle$ at each plume location

tail of the concentration probability distributions. To that purpose, we exhibit in Fig. 7 the exceedance distribution functions, $1 - F(c/C)$, for the same plume locations shown in Fig. 6 for dispersion in the URB01 obstacle array. The exceedance distribution functions have been plotted on a logarithmic scale in order to emphasize the upper tails. Figure 7 indicates that the clipped-gamma distribution predicts generally the upper tail very well. However, near the source, it appears that the upper tail of the modeled distribution falls off more rapidly than the

measured distribution. The largest discrepancy occurs along the mean-plume centerline at row 4.5 where the clipped-gamma distribution exhibits a considerably shorter upper tail than the observed concentration probability distribution, implying that the model under-predicts the probability of occurrence of large concentrations here.

As another example, Figs. 8 and 9 exhibit the measured CDFs and EDFs, respectively, of the normalized concentration χ/C. These were obtained at four different downstream locations at the fixed height $z/H = 0.5$ along the centerline of the plume dispersing in the URB04 obstacle array, with the source located in quadrant C. Additionally, these figures show the predictions provided by the clipped-gamma distribution (solid line), which were generated using the measured mean-square concentration $\langle (\chi/C)^2 \rangle$ obtained at each of these plume locations. Again, it can be seen that the clipped-gamma distribution provides excellent approximations for the shape of the measured concentration probability distributions over the entire range of concentration values. More importantly, the extent of the upper tails of the concentration probability distributions is generally predicted very well using the clipped-gamma distribution (and, only at row 4.5, does the model distribution under-predict the upper tail of the measured concentration probability distribution).

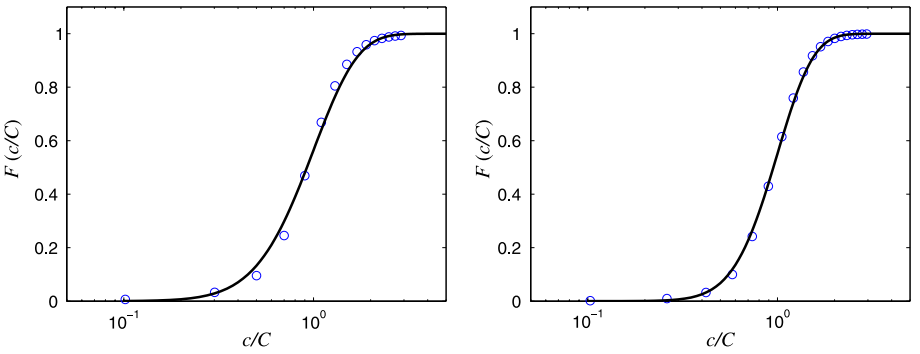

(a) Plume centerline at row 2.5 **(b)** Plume centerline at row 3.5

(c) Plume centerline at row 4.5 **(d)** Plume centerline at row 9.5

Fig. 8 Cumulative distribution function (CDF), $F(c/C)$, of the normalized concentration measured at various receptor positions at height $z/H = 0.5$ along the centerline of a plume dispersing in the URB04 obstacle array, with the source in quadrant C. The plot also includes the prediction of the concentration CDF given by the clipped-gamma distribution (*solid line*), which was generated using the observed normalized mean-square concentration $\langle (\chi/C)^2 \rangle$ at each plume location

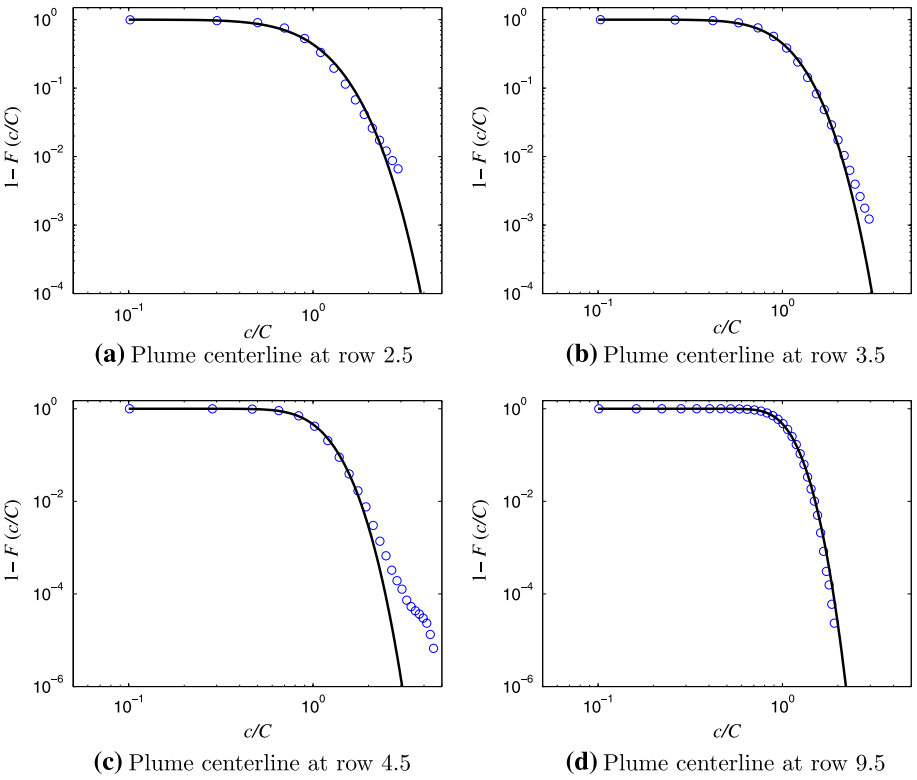

Fig. 9 Exceedance distribution function (EDF), $1 - F(c/C)$, of the normalized concentration measured at various receptor positions at height $z/H = 0.5$ along the centerline of a plume dispersing in the URB04 obstacle array, with the source in quadrant C. The plot also includes the prediction of the concentration EDF given by the clipped-gamma distribution (*solid line*), which was generated using the observed normalized mean-square concentration $\langle(\chi/C)^2\rangle$ at each plume location

With increasing downwind distance from the source, the concentration values become increasingly concentrated at $\chi/C \approx 1$ (and the upper and lower tails of the probability distribution become shorter and shorter), implying that the contaminant material in the plume is becoming more and more well mixed (leading to a homogenization of the in-plume structure). This feature in the measured concentration probability distribution conforms well with the approximation provided by the clipped-gamma distribution. A comparison of Fig. 6 with Fig. 8 shows that a plume dispersing in the random-height obstacle array (URB04) evolves faster towards a perfectly-mixed state (with $\chi/C \to 1$, so $F(c/C) \to H(c/C - 1)$ where $H(\cdot)$ is the unit step function) than a plume dispersing in the uniform-height obstacle array (URB01). This implies that the stirring of the plume material in the random-height obstacle array is more vigorous than in the uniform-height obstacle array, leading to a faster decrease in the concentration variance and a faster approach to the perfectly-mixed plume state.

6 Discussion and conclusion

This paper investigates the probability law of concentration for plumes dispersing in various idealized obstacle arrays (built-up environment). The form of the concentration PDF was

studied by examining the relationships between various normalized higher-order concentration moments. A large and comprehensive concentration data set, obtained from a series of water-channel measurements of near-field plume dispersion, was used for this purpose. For the present study, we extracted a large number of concentration time series from a number of different experiments involving various obstacle arrays (e.g., various arrays of cubical and non-cubical obstacles in aligned and staggered arrangements with uniform, random and alternating heights).

The key conclusions revealed by this analysis can be summarized as follows. A remarkably robust feature of all the concentration data was the observed collapse of the third- and fourth-order normalized concentration moments on the second-order normalized concentration moment. This collapse suggests that the normalized third- and fourth-order concentration moments can be represented by universal functions $F_3\left(\langle(\chi/C)^2\rangle\right)$ and $F_4\left(\langle(\chi/C)^2\rangle\right)$, respectively, in the sense that F_3 and F_4 appear to be independent (approximately or better) of the geometry of the obstacle array. Indeed, all the third- and fourth-order concentration moment data obtained from plume dispersion in the various obstacle arrays appear to fit on universal curves described by F_3 and F_4, respectively (although the exact theoretical forms for F_3 and F_4 are not known). Moreover, the collapse of the various concentration moments was found to be exactly the same as that observed in the CONFLUX concentration data for open-terrain plumes. This remarkable collapse suggests that the concentration PDF of plumes dispersing in either a built-up or open-terrain environment can be described adequately by at most two parameters (namely, a location parameter which can be chosen to be the mean concentration and a scale parameter which can be chosen to be the root-mean-square concentration or, equivalently, the concentration standard deviation). Finally, the two-parameter probability law of concentration appears to be universal, possibly valid for dispersion in all forms of environments (e.g., open terrain, urban areas).

We found that the observed universal relationships between the various higher-order normalized concentration moments can be adequately approximated using a two-parameter clipped-gamma distribution. Furthermore, the general shape of the observed concentration probability distribution is well approximated using the clipped-gamma distribution. More specifically, the form of both the lower and upper tails of the measured concentration probability distribution for urban and open-terrain plumes is well predicted using the clipped-gamma probability law.

At first, these conclusions seem rather surprising in view of the fact that it is known that large groups of obstacles (characteristic of a built-up environment) can have a profound effect on the mean concentration in a dispersing plume, in comparison to plume dispersion over open terrain [25–27]. In an obstacle array, non-Gaussian distributions of mean concentration are possible due to the splitting of plumes into two by the horseshoe vortex that may form around the base of an obstacle. There may be an effective lifting of the mean-plume centroid caused by deflection of mean flow streamlines over an array of obstacles. The trajectory of the mean plume centerline in the lateral direction may be offset from the direction of the mean wind aloft due to crosswind channeling of the flow in the array of obstacles. In certain circumstances, channeling of the flow along array passages may inhibit the lateral spread of the mean plume. Alternatively, topological diffusion of the plume due to streamline divergence can lead to an enhanced lateral mean plume spread, whereas rapid vertical mixing in the recirculating wakes behind obstacles may lead to an enhanced vertical mean plume spread. The mean concentration pattern can be moulded by the entrainment of plume material into the re-circulating flow regions in the wakes of obstacles, providing secondary sources for dispersion.

Similarly, the dispersion of pollutant material in an array of buildings can have a significant effect on the concentration variance field. For example, Yee and Biltoft [14] demonstrated that the second moment of concentration (or, concentration variance) in a plume dispersing through an array of obstacles is reduced, relative to that observed in a comparable plume dispersing over open terrain. This reduction in the concentration variance is the consequence of two physical processes in the dispersion: namely, (1) a significant reduction in the meandering of the instantaneous plume in an obstacle array (relative to an open-terrain plume) due to an observed increase in the lateral spreads of the plume and a reduction in the scale of turbulence between the obstacles in the array, and (2) a significant reduction in concentration variance of the in-plume fluctuations in the array plume (in comparison to the open-terrain plume) owing to the enhanced small-scale mixing of the plume material in the high intensity turbulence that is characteristic of the flow within an obstacle array.

In spite of the significant modifications in the structure of a plume dispersing in an obstacle array when compared to an open-terrain plume, the modifications manifest themselves in their effects on the first- and second-order concentration moments (or, equivalently, on the mean concentration and concentration variance). Interestingly, Fig. 5 seems to suggest that despite the fact that an obstacle array has a significant effect on the first two moments of the concentration, the relationships of the third- and fourth-order normalized concentration moments to the second-order normalized concentration moment in an array plume are exactly the same (approximately or better) as those for an open-terrain plume.

It appears that the plume concentration fluctuation structure in an obstacle array is the same as that which would be observed in an open-terrain plume, but at a much greater distance downwind when the instantaneous plume has grown to fill the mean-plume width (hence, dramatically reducing the contribution of large-scale meander to the concentration fluctuations) and when the continual molecular mixing has had a chance to smooth out the in-plume fluctuations. Indeed, the latter effect on the structure of an open-terrain plume is indistinguishable from the effect of the more rapid, homogeneous mixing in an array plume resulting from the extra straining and shearing motions in the small-scale, high-intensity turbulence that is characteristic of an urban canopy flow.

More specifically, the two physical processes responsible for micro-mixing in a dispersing plume (whether in open or urban terrain) are exactly the same; stirring by the turbulent velocity field and mixing by molecular diffusion which determine the "texture" of the plume [28,29]. In turn, the plume "texture" determines the relationships between the concentration moments and the probability law of concentration. The only difference is that the extra straining and shearing motions in urban canopy turbulence facilitate stirring and reduce the time scale to achieve molecular mixing. The more vigorous mixing of the plume material in an urban canopy reduces the concentration variance (or, equivalently, the mean-square concentration). However, as the concentration variance is reduced, the third-order and fourth-order concentration moments are not changed independently of the change in the mean-square concentration. Rather, the third-order and fourth-order concentration moments are simply "moved" along the curves $F_3\left(\langle\,(\chi/C)^2\,\rangle\right)$ and $F_4\left(\langle\,(\chi/C)^2\,\rangle\right)$ to reflect the new (reduced) value of $\langle\,(\chi/C)^2\,\rangle$ resulting from the better mixing in the urban canopy. This explains why the concentration moment relationships measured in an array plume are identical (approximately or better) to those measured in an open-terrain plume. In hindsight, the universality of the concentration moment relationships and the probability law of concentration should not be too surprising.

An important implication for the results of this paper is as follows. The two-parameter clipped-gamma probability law of concentration can be used in conjunction with predictive

models for the mean concentration and concentration variance in urban plumes to provide a prognostic probabilistic model for the assessment of actual or potential hazards (toxicity, flammability, malodour), resulting from the dispersion of pollutant plumes in built-up areas. Preliminary models that can be used for the prediction of the mean concentration and concentration variance of plumes dispersing in urban areas have begun to appear recently (see e.g., Hsieh et al. [30]; Milliez and Carissimo [31]; Wang et al. [32,33]). A full realization of this probabilistic modeling of concentration fluctuations in plumes dispersing in an urban environment has been described by Yee and Wang [34].

Acknowledgement This work has been partially supported by Chemical Biological Radiological Nuclear Research and Technology Initiative (CRTI) program under project number CRTI-02-0093RD.

References

1. Griffiths RF, Megson LC (1984) The effect of uncertainties in human toxic response on hazard range estimation for ammonia and chlorine. Atmos Environ 18:1195–1206
2. ten Berge WF, Zwart A, Appelman LM (1986) Concentration-time mortality response relationships of irritant and systemically acting vapours and gases. J Hazard Mater 13:301–309
3. Yee E (1999) An impact-effect mathematical model incorporating the influence of exposures to fluctuating concentrations in a dispersing plume of pollutant in the atmosphere. J Expo Anal Environ Epidemiol 9:300–311
4. Birch AD, Brown D, Dodson M, Thomas JR (1978) The turbulent concentration field of a methane jet. J Fluid Mech 88:431–449
5. Chatwin PC (1982) The use of statistics in describing and predicting the effects of dispersing gas clouds. J Hazard Mater 6:213–230
6. Csanady GT (1973) Turbulent diffusion in the environment. D. Reidel, Dordrecht
7. Hanna SR (1986) The exponential probability density function and concentration fluctuations in smoke plumes. Boundary-Layer Meteorol 37:89–106
8. Lewellen WS, Sykes RI (1986) Analysis of concentration fluctuations from lidar observations of atmospheric plumes. J Clim Appl Meteorol 25:1145–1154
9. Sawford BL (1987) Conditional concentration statistics for surface plumes in the atmospheric boundary layer. Boundary-Layer Meteorol 38:209–223
10. Mylne KR, Mason PJ (1991) Concentration fluctuation measurements in a dispersing plume at a range of up to 1000 m. Q J R Meteorol Soc 117:177–206
11. Yee E (1990) The shape of the probability density function of short-term concentration fluctuations of plumes in the atmospheric boundary layer. Boundary-Layer Meteorol 51:269–298
12. Yee E, Wilson DJ, Zelt BW (1993) Probability distributions of concentration fluctuations of a weakly diffusive passive plume in a turbulent boundary layer. Boundary-Layer Meteorol 64:321–354
13. Lewis DM, Chatwin PC (1995) A new model PDF for contaminants dispersing in the atmosphere. Environmetrics 6:583–593
14. Yee E, Biltoft CA (2004) Concentration fluctuation measurements in a plume dispersing through a regular array of obstacles. Boundary-Layer Meteorol 111:363–415
15. Gailis RM, Hill A (2006) A wind-tunnel simulation of plume dispersion within a large array of obstacles. Boundary-Layer Meteorol 119:289–338
16. Yee E, Gailis RM, Hill A, Hilderman T, Kiel D (2006) Comparison of wind-tunnel and water-channel simulations of plume dispersion through a large array of obstacles with a scaled field experiment. Boundary-Layer Meteorol 121:389–432
17. Klein P, Leitl B, Schatzmann M, Young D (2008) Concentration fluctuations in a downtown urban area—analysis of concentration data from the Joint Urban 2003 full-scale and wind tunnel measurements. In: Proceedings of 15th joint conference on the applications of air pollution meteorology with the A&WMA, New Orleans, LA, Paper AIRPOL 6.2
18. Hilderman T, Chong R (2007) A laboratory study of momentum and passive scalar transport and diffusion within and above a model urban canopy. DRDC Suffield CR 2008-025, Defence R&D Canada – Suffield, Ralston, Alberta, Canada
19. Yee E, Chan R (1997) A simple model for the probability density function of concentration fluctuations in atmospheric plumes. Atmos Environ 31:991–1002

20. Yee E, Kosteniuk PR, Chandler GM, Biltoft CA, Bowers JF (1993) Statistical characteristics of concentration fluctuations in dispersing plumes in the atmospheric surface layer. Boundary-Layer Meteorol 65:69–109
21. Yee E, Kosteniuk PR, Chandler GM, Biltoft CA, Bowers JF (1993) Recurrence statistics of concentration fluctuations in plumes within a near-neutral atmospheric surface layer. Boundary-Layer Meteorol 66:127–153
22. Yee E, Chan R, Kosteniuk PR, Chandler GM, Biltoft CA, Bowers JF (1994) Experimental measurements of concentration fluctuations and scales in a dispersing plume in the atmospheric surface layer obtained using a very fast-response concentration detector. J Appl Meteorol 33:996–1016
23. Yee E, Chan R, Kosteniuk PR, Chandler GM, Biltoft CA, Bowers JF (1994) Measurements of level-crossing statistics of concentration fluctuations in plumes dispersing in the atmospheric surface layer. Boundary-Layer Meteorol 73:53–90
24. Yee E, Chan R, Kosteniuk PR, Chandler GM, Biltoft CA, Bowers JF (1995) The vertical structure of concentration fluctuation statistics in plumes dispersing in the atmospheric surface layer. Boundary-Layer Meteorol 76:41–67
25. Jerram N, Perkins RJ, Fung JCH, Davidson MJ, Belcher SE, Hunt JCR (1995) Atmospheric flow through groups of buildings and dispersion from localised sources. In: Cermak JE, Davenport AG, Plate EJ, Domingos X (eds) Wind climate in cities. Kluwer, Dordrecht pp 109–130
26. Davidson MJ, Mylne KR, Jones CD, Phillips JC, Perkins RJ, Fung JCH, Hunt JCR (1995) Plume dispersion through large groups of obstacles—a field investigation. Atmos Environ 29:3245–3256
27. Macdonald RW, Griffiths RF, Hall DJ (1998) A comparison of results from scaled field and wind-tunnel modeling of dispersion in arrays of obstacles. Atmos Environ 32:3845–3862
28. Yee E, Chan R, Kosteniuk PR, Chandler GM, Biltoft CA, Bowers JF (1995) Multiscaling properties of concentration fluctuations in dispersing plumes revealed using an orthonormal wavelet decomposition. Boundary-Layer Meteorol 77:173–207
29. Yee E (1998) High-resolution measurements of the detailed structure and texture in contaminant plumes dispersing in the atmospheric surface layer. Recent Res Dev Phys Fluids 1:1–23
30. Hsieh KJ, Lien FS, Yee E (2007) Numerical modeling of passive scalar dispersion in an urban canopy layer. J Wind Eng Ind Aerodyn 95:1611–1636
31. Milliez M, Carissimo B (2008) Computational fluid dynamical modeling of concentration fluctuations in an idealized urban area. Boundary-Layer Meteorol 127:241–259
32. Wang BC, Yee E, Lien FS (2008) Study of turbulent passive scalar dispersion within a regular array of obstacles. In: Friedrich R, Adams NA, Eaton JK, Humphrey JAC, Kasagi N, Leschziner MA (eds) Proceedings of the 5th international symposium on turbulent shear flow phenomena, Munich, Germany, pp 333–338
33. Wang BC, Yee E, Lien FS (2008) Numerical study of dispersing pollutant clouds in a built-up environment. Int J Heat Fluid Flow (Accepted for publication)
34. Yee E, Wang BC (2009) Quantitative probabilistic model for urban dispersion. In: 8th symposium on the urban environment, Phoenix, AZ, Paper J18.1, 12 pp